Cellular/Molecular

The RCK2 Domain Uses a Coordination Site Present in Kir Channels to Confer Sodium Sensitivity to Slo2.2 Channels

Zhe Zhang,[1] **Avia Rosenhouse-Dantsker,**[2] **Qiong-Yao Tang,**[1] **Sergei Noskov,**[3] **and Diomedes E. Logothetis**[1]

[1]Department of Physiology and Biophysics, Virginia Commonwealth University, School of Medicine, Richmond, Virginia 23298, [2]Department of Medicine, University of Illinois at Chicago, Chicago, Illinois 60612, and [3]Institute of Biocomplexity and Informatics, Department of Biological Sciences, University of Calgary, Calgary, Alberta T2N 1N4, Canada

Slo2 Na^+-activated potassium channels are widely expressed in neurons and other cells, such as kidney, heart, and skeletal muscle. Although their important physiological roles continue to be appreciated, molecular determinants responsible for sensing intracellular Na^+ remain unknown. Here we report identification of an Na^+ regulatory site, similar to an Na^+ coordination motif described in Kir channels, localized in the RCK2 domain of Slo2.2 channels. Molecular simulations of the homology-modeled Slo2.2 RCK2 domain provided structural insights into the organization of this Na^+ coordination site. Furthermore, free energy calculations reproduced the experimentally derived monovalent cation selectivity. Our results suggest that Slo2.2 and Kir channels share a similar mechanism to coordinate Na^+. The localization of an Na^+ sensor within the RCK2 domain of Slo2.2 further supports the role of RCK (regulators of conductance of K^+) domains of Slo channels in coupling ion sensing to channel gating.

Introduction

The Na^+-activated potassium channel (K_{Na}) currents were first recorded in guinea pig ventricular myocytes (Kameyama et al., 1984). The open probability of these highly selective K^+ channels was found to be steeply dependent on the Na^+ concentration (Kameyama et al., 1984). The K_{Na} channel Slo2.2 [or Slack (for "sequence like a calcium-activated K^+")] is a member of the Slo2 gene family (Yuan et al., 2003). There are two N-terminal splice variants of the Slack mRNA, a shorter Slack-A and a longer Slack-B. The rSlack-B gene encodes a 1237 aa protein, which can form homomeric channels but can also coassemble with another homologous protein named Slick [for "sequence like an intermediate conductance K channel" (Slo2.1)] to form heteromeric channels (Bhattacharjee et al., 2003; Brown et al., 2008; Chen et al., 2009). The full-length rat Slick gene encodes a protein of 1142 aa that shares 74% sequence identity to the rat Slack protein. Sodium-activated K^+ channels (K_{Na} channels) are members of a family of high-conductance potassium ion channels. Their amino acid sequence contains six putative membrane-spanning domains, a P-region between predicted transmembrane domains 5 and 6, and an extensive C-terminal region. The C-terminal region of both Slick and Slack is predicted to encode two RCK (regulators of conductance of K^+) domains, similar to the Slo1 gene that encodes the large-conductance calcium-activated potassium channel (Jiang et al., 2002a,b). Thus far, the molecular determinants of the sodium regulatory site(s) of the Slack channel remain unknown.

Sodium-activated potassium channels are widely expressed in the CNS and in heart (Egan et al., 1992; Bhattacharjee et al., 2002). K_{Na} channels may play an important role in synaptic transmission (Nanou and El Manira, 2007; Nanou et al., 2008), in the modulation of the action-potential waveform (Yang et al., 2007; Gao et al., 2008), and in the responses of excitable cells to hypoxia and ischemia (Dryer, 1994).
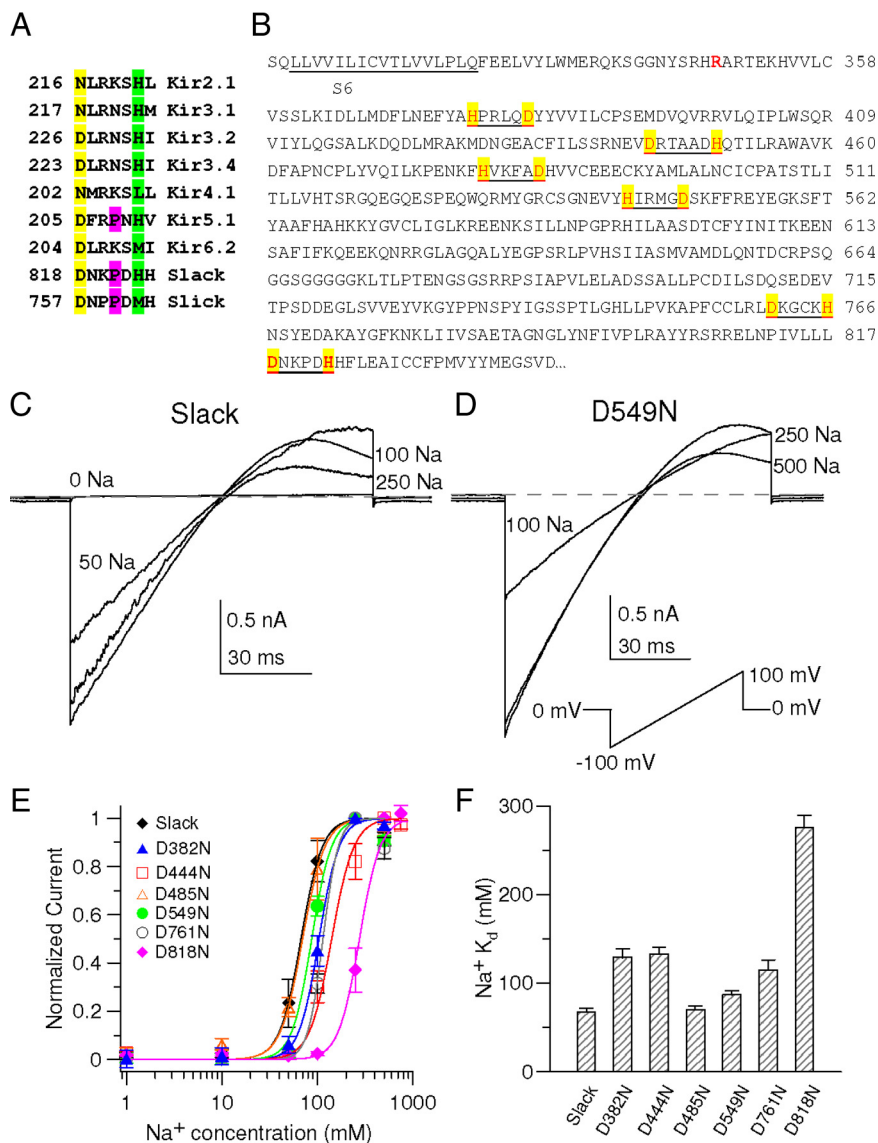
Native G-protein-sensitive inwardly rectifying K^+ (GIRK) (K_{Ach} or Kir3) channels are also activated by Na^+ (Sui et al., 1996). Na^+ activation of Kir3 channels is limited to the neuronal Kir3.2 (GIRK2) and the cardiac Kir3.4 (GIRK4) subunits. Chimeras between Kir3.1 and Kir3.2 or Kir3.4 identified a critical Asp residue (GIRK2–D226 and GIRK4–D223) as a sodium regulatory site in the Kir3.2 channel (Ho and Murrell-Lagnado, 1999a; Zhang et al., 1999). The reverse equivalent mutation N217D in the Kir3.1 channel and N216D in the Kir2.1 (IRK1) channel conferred sodium sensitivity to these channels (Ho and Murrell-Lagnado, 1999b; Zhang et al., 1999). Molecular dynamics (MD) simulations using the structure of Kir3.1 combined with experimental tests revealed that the Asp coordinates the Na^+ ion as part of a loop structure with the aid of a His side chain as well as backbone carbonyls of two other residues (Rosenhouse-Dantsker et al., 2008). Moreover, Kir5.1 that possesses the DXRXXH motif was also shown to be Na^+ sensitive.

A


```
216  NLRKSHL  Kir2.1
217  NLRNSHM  Kir3.1
226  DLRNSHI  Kir3.2
223  DLRNSHI  Kir3.4
202  NMRKSLL  Kir4.1
205  DFRPNHV  Kir5.1
204  DLRKSMI  Kir6.2
818  DNKPDHH  Slack
757  DNPPDMH  Slick
```

B

```
SQLLVVILICVTLVVLPLQFEELVYLWMERQKSGGNYSRHRARTEKHVVLC  358
s6
VSSLKIDLLMDFLNEFYAHPRLQDYYVVILCPSEMDVQVRRVLQIPLWSQR  409
VIYLQGSALKDQDLMRAKMDNGEACFILSSRNEVDRTAADHQTILRAWAVK  460
DFAPNCPLYVQILKPENKFHVKFADHVVCEEECKYAMLALNCICPATSTLI  511
TLLVHTSRGQEGQESPEQWQRMYGRCSGNEVYHIRMGDSKFFREYEGKSFT  562
YAAFHAHKKYGVCLIGLKREENKSILLNPGPRHILAASDTCFYINITKEEN  613
SAFIFKQEEKQNRRGLAGQALYEGPSRLPVHSIIASMVAMDLQNTDCRPSQ  664
GGSGGGGGGKLTLPTENGSGSRRPSIAPVLELADSSALLPCDILSDQSEDEV  715
TPSDDEGLSVVEYVKGYPPNSPYIGSSPTLGHLLPVKAPFCCLRLDKGCKH  766
NSYEDAKAYGFKNKLIIVSAETAGNGLYNFIVPLRAYYRSRRELNPIVLLL  817
DNKPDHHFLEAICCFPMVYYMEGSVD...
```

C

Slack

D

D549N

E

F

Figure 1. Screening for potential Na$^+$ binding site(s) in the C terminus of the Slack channel. **A**, Comparisons of the Na$^+$ coordination site in Kir channels with the analogous region in Slack and Slick channels. **B**, Based on the Na$^+$ coordination site identified in the C terminus of Kir channels, there are six potential similar Na$^+$ binding sites in the Slack channel. **C, D**, Typical current traces recorded in the inside-out patch configuration for Slack and D549N mutants. **E**, Hill equation fitted data of the Na$^+$ dose dependence of wild-type Slack (K_d of 67 ± 3.8 mM, n = 3.98), D382N (K_d of 129 ± 9.8 mM, n = 3.9), D444N (K_d of 133 ± 4.6 mM, n = 4 fixed), D485N (K_d of 70.3 ± 4 mM, n = 3.9), D549N (K_d of 87.3 ± 4.5 mM, n = 3.93), D761N (K_d of 114.8 ± 11.3 mM, n = 3.9), and D818N (K_d of 276 ± 13.6 mM, n = 4.0). **F**, Summary of K_d values for wild-type and all Slack channel mutants tested.

In the present study, we investigated whether the Na$^+$ coordination motif found in Kir channels also exists in Slack channels. By screening the Slack-B channel C terminus with the Kir Na$^+$ coordination motif sequence, we identified an Asp residue (D818) in the Slack RCK2 domain, the mutation of which dramatically decreased the sodium sensitivity of Slack channels. Additional mutagenesis scanning experiments revealed the His (H823) residue corresponding to the His residue in the Kir motif that also critically contributed to the Na$^+$ sensitivity of Slack channels. Molecular simulations and free energy calculations reproduced the experimentally derived monovalent cation selectivity. These results indicate that a conserved Na$^+$ coordination site is shared by two different types of K$^+$ channels, the K$_{Na}$ and Kir channels.

Materials and Methods

Oocyte isolation and culture. Stage VI *Xenopus laevis* oocytes were harvested and used for cRNA injection as described previously (Rosenhouse-Dantsker and Logothetis, 2006). Slack and Slick mutant cRNAs were prepared at a concentration of ~1 μg/μl, and each oocyte was injected with 50 nl of cRNA. Currents were recorded within 3–5 d.

Constructs and mutations. The Slack-B construct (GenBank accession number NP 942057) was a gift from Dr. Kaczmarek (Yale University School of Medicine, New Haven, CT). Slack mutations were made following previously published procedures (Jin et al., 2002).

Electrophysiology. Currents were recorded in the inside-out patch configuration using an EPC 9 amplifier (HEKA) and the Pulse fit program (HEKA). We observed current rundown in ~50% of excised inside-out patches. All currents were recorded within 30 s after patch excision to minimize significant rundown (Tamsett et al., 2009), and only patches that did not show rundown were included in the analysis. Patch-clamp recording pipettes were made from borosilicate capillary tubes (PG10150-4; World Precision Instruments) and had resistances of 1–3 MΩ. Gigaohm seals were formed in ND96K–EGTA solution [in mM: 90 KCl, 20 HEPES-K, and 50 EGTA-K-02/06M (200 mM EGTA and 600 mM KOH), pH 7.4]. The standard pipette/extracellular solution was also ND96K–EGTA. Different bath solutions (BS) were used. For screening and scanning Na$^+$ sensitivity of Slack mutations, BS1 contained the following (in mM): 90 KCl, 20 HEPES-K, 50 EGTA-K-02/06M, and 0–1000 NaGlu. For testing the Na$^+$ sensitivity of constructs in the absence of Cl$^-$, BS2 contained the following (in mM): 90 mM KGlu, 20 HEPES-K, 50 EGTA-K-02/06M, and 0–1000 NaGlu. For testing sensitivity of constructs to chloride, BS3 contained the following (in mM): 90 mM KGlu, 20 HEPES-K, 50 EGTA-K-02/06M, and 0–500 choline chloride. Experiments were performed at 22–25°C. Salts of the compounds mentioned were obtained from Sigma.

Single-channel analysis. Amplitude histograms were measured, idealized, and fitted with a Gaussian function using the software ANA.EXE. The open probability (P_o) of the channels was calculated using the area under each peak (aj) at each current level (j) in the histogram along with the number of channels (N) as follows:

$$P_o = \frac{\sum_{j=0}^{N}(j * aj)}{n \times \sum_{j=0}^{N} aj}. \tag{1}$$

Homology modeling. A segment that includes residues 243–321 of the crystallographic structure of the RCK domain from the *Escherichia coli* K$^+$ channel (Protein Data Bank identification number 1id1) (Jiang et al., 2001) was used as the basis for the homology model of the segment of Slo2.2 that includes residues 778–865. The resolution of the crystallographic structure (Protein Data Bank identification number 1id1) was 2.4 Å, and the overall similarity (identity, strong and weak similarity) between the sequences of the segments of the RCK domain (residues

243–321) and Slo2.2 (residues 778–865) was 56%. The basic model was constructed using the protein homology/analogy recognition engine QuickPhyre (Bennett-Lovsey et al., 2008). The homology model was then minimized using the Steepest Descent and the adopted-basis Newton Raphson algorithms as implemented in CHARMM version 32 (Brooks et al., 1983). The final orientation of the side chains in the homology model was obtained after minimization in the presence of sodium.

Molecular modeling. The c35b1 version of the CHARMM program (Brooks et al., 1983) was used to run MD simulations for the Kir3.1N217D cytosolic domain (Protein Data Bank identification number 19NP) and the homology modeled domain of Slo2.2. The Na$^+$ ion was introduced at the binding pocket identified in a previous study in Kir channels (Ho and Murrell-Lagnado, 1999a; Rosenhouse-Dantsker et al., 2008). The simulation box contained one protein with one bound Na$^+$ solvated by a 100 mM NaCl aqueous salt solution, comprising a total of ~48,000 atoms. The CHARMM–GUI interface was used to build all simulation systems (Jo et al., 2009). All simulations were performed at constant pressure (1 atmospheric unit) and constant temperature with periodic boundary conditions (Feller et al., 1995). Electrostatic interactions were treated using a particle mesh Ewald algorithm (Essmann et al., 1995). All systems were equilibrated for 1.5 ns and then subjected to 10 ns production runs. The analysis of root mean square (RMS) fluctuations indicates that structures for wild-type and mutant proteins were stable for the entire simulation time. The SCWRL 4.0 was used to introduce side-chain replacements for construction of mutated amino acid residues (Krivov et al., 2009). To ensure optimal packing for the mutated residue, 2 ns of the reequilibrating MD simulations were performed in the presence of weak harmonic constraints (1 kcal/mol/Å^2) on the backbone before production runs.

Free energy simulations: evaluation of relative ion binding affinities. Free energy perturbation (FEP) simulations to evaluate the absolute free energy of ion uncharging and the relative free energy for site specificity of the sequence Li$^+$, Na$^+$, K$^+$ were performed using the CHARMM PERT command for the Kir3.1N217D and the Slo2.2 cytosolic domains as well as for the Slo2.2 mutants D818E, D818N, and D818R using a previously developed protocol (Caplan et al., 2008; Noskov and Roux, 2008). A thermodynamic coupling parameter λ varying between 0 and 1 was used to alchemically transform Na$^+$ into a different ion type (K$^+$ or Li$^+$), and 11 intermediate windows were used to go from 0 to 1 in increments of 0.1. A total of 22 windows with 500 ps each were run to obtain converged estimates on the relative free energies. The relative free energies used to characterize the binding site selectivity are as follows:

$$\Delta\Delta G_{ij} = \Delta G_{ij}^{site} - \Delta G_{ij}^{bulk}, \qquad (2)$$

where ΔG_{ij}^{site} is the difference in free energies of binding to the site between ion i and j, and ΔG_{ij}^{bulk} is the difference in free energies of hydration between ion i and ion j. The positive sign in the relative free energy refers to the preference by the site for ion i. The reference values for the absolute free energy of Li$^+$, Na$^+$, and K$^+$ uncharging (G_{elec}^{bulk}) in the bulk water was estimated to be −113.1, −89.5, and −71.9 kcal/mol, respectively. These numbers are reported for simulations with periodic boundary conditions and have to be corrected for the presence of interfacial potential (correction of approximately −10 kcal/mol for the model used) to compare directly with experimental measurements. It should be noted that the relative free energies are insensitive to this correction as a result of the
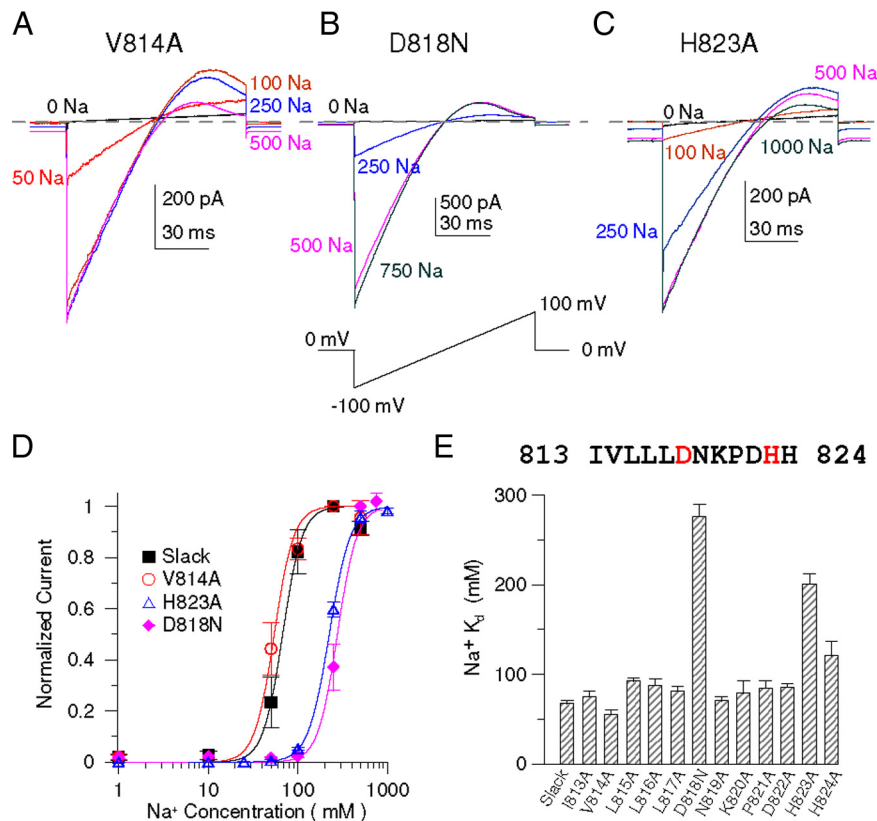
Figure 2. Alanine scanning Na$^+$ sensitivity of 11 residues around D818. ***A–C***, Samples (V814A, D818N, and H823A) of typical present traces recorded with a ramp protocol from −100 to +100 mV in the inside-out patch configuration. The bath solution was BS1. ***D***, Hill equation fits of the Na$^+$ dose–response data of V814A. ***E***, Amino acid sequence around the D818 residue of Slack used for Ala scanning and summary of the Na$^+$ sensitivity K_d values for Slack mutations around the D818 residue.

cancellation of this term. The reference values for relative free energy differences in the bulk for the model used in our study are $\Delta\Delta G$(Na$^+$ → K$^+$) = 18.01 kcal/mol (FEP simulation) or $\Delta\Delta G$(Na$^+$ → K$^+$) = 18.01 kcal/mol (as a difference in absolute free energies) and $\Delta\Delta G$(Na$^+$ → Li$^+$) = −23.4 kcal/mol. All parameters as well as the development protocol have been published previously (Caplan et al., 2008). This approach to absolute and relative free energy computations is rooted in equilibrium thermodynamics of ion solvation but has been proven useful in many studies of ion permeation (Luzhkov and Aqvist, 2001; Noskov et al., 2004; Luzhkov et al., 2006). The weighted histogram analysis method was used to post-process the FEP calculation data (Kumar et al., 1992; Souaille and Roux, 2001).

Results

A common Na$^+$ coordination site used by both Kir and Slo2.2 channels.

Figure 1*A* shows a seven residue sequence of the Kir Na$^+$ coordination site that uses the side chains of the amino acid residues Asp and His at positions 1 and 6 separated by 4 aa, one of which is a highly conserved basic residue in position 3 (R). Three Kir channels (Kir3.2, Kir3.4, and Kir5.1) that possess the motif DXRXXH were shown to be Na$^+$ sensitive, whereas others (Kir2.1 and Kir3.1) could be made Na$^+$ sensitive by engineering the motif through mutagenesis (Zhang et al., 1999; Rosenhouse-Dantsker et al., 2008). Six potential sites in the C terminus of the Slack channel were similar to the Kir Na$^+$ coordination motif, including an aspartate and a histidine separated by four to five residues, with a positively charged residue (R/K) between these two residues (Fig. 1*B*). In view of the flexibility of the CD loop that includes the sodium-binding motif in Kir channels, the pos-
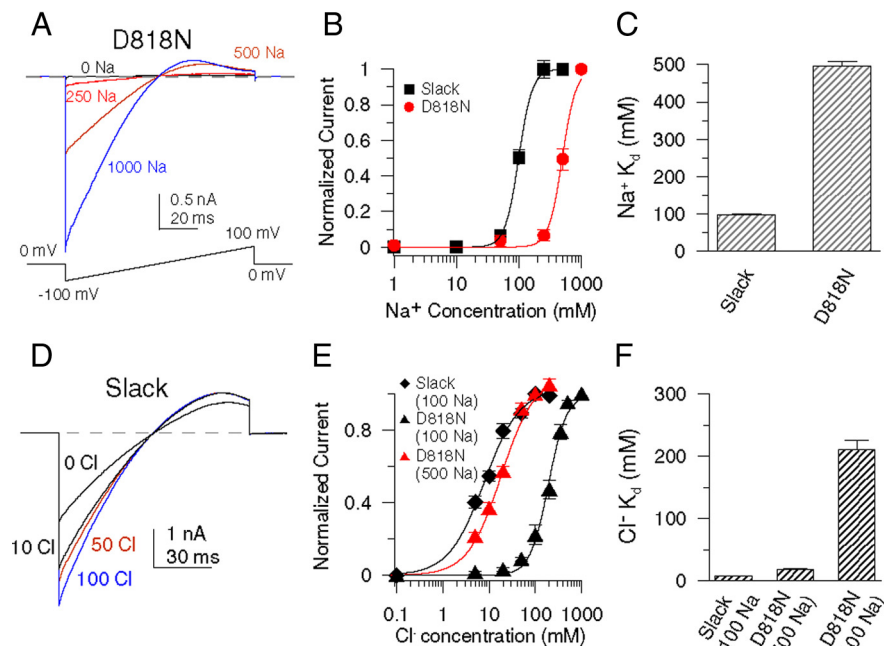
Figure 3. The change in Na$^+$ sensitivity of D818N is independent of Cl$^-$. ***A***, Typical current traces recorded in the inside-out patch configuration for D818N. The bath solution was BS2. ***B***, Na$^+$ dose–response for the wild-type Slack channel and the D818N mutant. Data were fitted with the Hill equation. ***C***, Summary of K_d values for the wild-type Slack (K_d of 99.1 ± 2.3 mM, n = 4.0) and the D818N mutant (K_d of 496.1 ± 11.7 mM, n = 4.0) in 0 mM Cl$^-$. ***D***, Typical current traces recorded in the inside-out patch configuration for Slack. The bath solution was BS3. ***E***, Cl$^-$ dose–response for the wild-type Slack channel and D818N mutant in 100 mM Na$^+$ and the D818N mutant in 500 mM Na$^+$. Data were fitted with the Hill equation. ***F***, Summary of K_d values for the wild-type Slack (K_d of 7.9 ± 0.8 mM, n = 1.12) and D818N (K_d of 210.7 ± 14.1 mM, n = 1.1) in 100 mM Na$^+$ and the D818N mutant (K_d of 18.2 ± 3.9 mM, n = 1.2) in 500 mM Na$^+$.

sibility of some deviation from the Kir sodium binding motif was taken into account during the design of the potential Na$^+$ binding sites in Slack. The Asp residues in these potential sites were neutralized to Asn to test whether these mutants affected the sensitivity of Slack channels to Na$^+$. We applied a ramp voltage protocol from −100 to +100 mV in inside-out patch-clamp recordings. Both currents from wild-type and mutant Slack channels exhibited sodium-dependent inward rectification attributable to voltage-dependent block by Na$^+$ (Fig. 1C,D). The current level at −90 mV in different Na$^+$ concentrations was used to assess the sensitivity of wild-type and mutant Slack channels to Na$^+$. The current levels measured in different Na$^+$ concentrations were normalized to the current level at 500 mM Na$^+$. Of the six putative Na$^+$-binding sites, four mutants, D382N, D549N, D444N, and D761N, decreased Slack channel sensitivity to Na$^+$ only slightly (K_d value increased less than twofold), whereas one mutant, D485N, showed the same sodium sensitivity as that of the wild-type Slack. In contrast, the D818N mutant dramatically decreased Slack sensitivity to Na$^+$ more than fourfold (Fig. 1E,F). Moreover, the D382ND818N double mutation did not show an additional decrease in sensitivity to Na$^+$ compared with D818N (data not shown), suggesting that D818 is a major determinant of Na$^+$ sensitivity in Slack channels.

We then asked whether the residues around D818 conformed to the Kir consensus site by performing alanine scanning mutagenesis and testing for effects on Na$^+$ sensitivity. We used a ramp protocol again and plotted the current values at −90 mV as a function of internal Na$^+$ concentration (Fig. 2D). Typical traces and normalized currents of V814A, D818N, and H823A fitted with the Hill equation are also shown (Fig. 2A–C). The D818A mutant was not functional (data not shown). Our results

illustrate that the K_d values of the sodium sensitivities of mutants neighboring the D818 residue were not significantly changed, with the exception of H823A (Fig. 2D,E). These results suggest that Slack channels share with Kir channels an Na$^+$ coordination site that is located in their RCK2 domain. The K820A mutation showed no effect on the Na$^+$ sensitivity of the channel. In Kir channels, mutation of an Arg residue corresponding to K820 greatly reduces channel activity. Sequence comparison suggests that this site is not intact in the Slick channel (Fig. 1A). Because the Slick channel is also Na$^+$ sensitive and the Slack channel retains a weak sodium dependence even after mutagenesis of the D818N/H823N sites, the existence of additional sodium binding sites is likely. Multiple sites for ion sensing are not surprising considering that the Slo1 Ca^{2+}-activated potassium channel, which belongs to same channel family, possesses three distinct Ca^{2+} binding sites that regulate its activity (Zeng et al., 2005).

Because Slack channels are also sensitive to Cl$^-$ and Na$^+$ and Cl$^-$ sensitivities show an intricate interdependence (Yuan et al., 2003), we investigated the Na$^+$ sensitivity of D818N in the absence of Cl$^-$. The 90 mM KCl was replaced by 90 mM KGlu in both our bath and pipette solutions. Typical current traces of D818N under this condition are shown in Figure 3A. Current levels recorded at −90 mV were normalized to currents recorded in 250 mM Na$^+$ (Slack) and 1000 mM Na$^+$ (D818N), respectively. Normalized currents were plotted and fitted by the Hill equation (Fig. 3B). Both the K_d value of the wild-type Slack channel and the D818N mutant were increased in the absence of Cl$^-$, however, the K_d value of D818N to Na$^+$ remained approximately fivefold higher than the value of the wild-type Slack channel (Fig. 3C). Our results suggest that the effect of D818N on the Na$^+$ sensitivity of the channel can operate independently of Cl$^-$. To assess a potential influence of the D818N on Cl$^-$ sensitivity, we performed inside-out patch-clamp recordings with different Cl$^-$ concentrations in the bath solution. Our results on wild-type Slack currents agree with previous reports (Yuan et al., 2003), showing that, in a 100 mM sodium solution, the K_d value of the Slack channel for Cl$^-$ was 7.9 ± 0.8 mM (data were fitted with the Hill equation; n = 1.1) (Fig. 3D–F). Not surprisingly, the D818N mutant also dramatically decreased the Cl$^-$ sensitivity of the channel. The K_d value of D818N for Cl$^-$ was 210 ± 14.3 mM in 100 mM Na$^+$, with a concomitant increase in the Hill coefficient factor (n = 1.9). This result suggests that disruption of an Na$^+$ regulatory site decreased Cl$^-$ sensitivity more than 25-fold, further underscoring the intricate coupling mechanism between Na$^+$ and Cl$^-$ sensitivities in Slack channels. Because Cl$^-$ sensitivity of Slack depends on Na$^+$ sensitivity, we further compared the effect of the D818N mutant on Cl$^-$ sensitivity in 500 mM Na$^+$ concentration, which provides a similar open probability for D818N as the open probability seen with the wild-type Slack channel in 100 mM Na$^+$. Our results show that the Cl$^-$ sensitivity of D818N was only approximately twofold less than the wild-type Slack channel in this condition. The K_d was
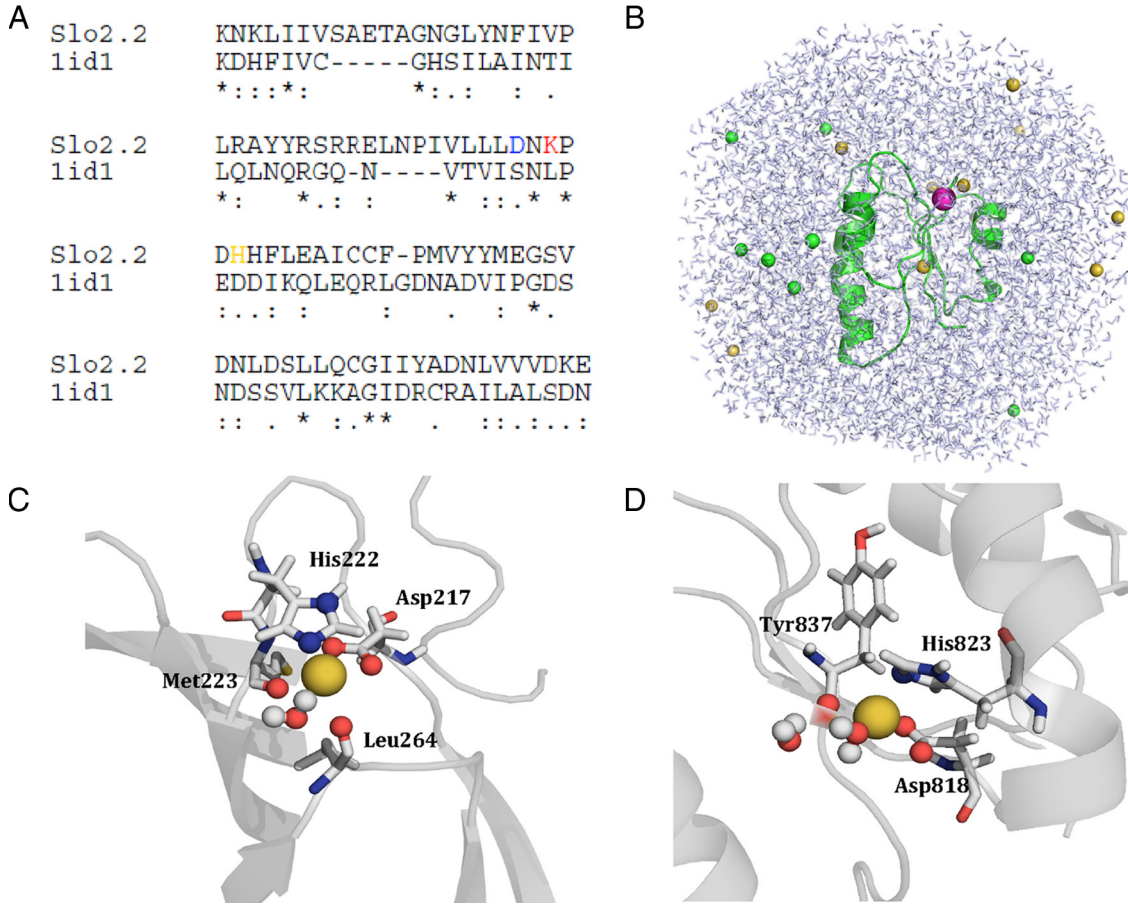
Figure 4. A model of the Na+ coordination site of Slack. **A**, Sequence alignment between the RCK domain from an *E. coli* K+ channel and the Slack used to construct a homology model. **B**, Example of the simulation system for MD studies of C terminus of Slack channel in explicit 100 mM NaCl (green and yellow spheres). Bound sodium ion shown in magenta. **C**, Simulated structure for the equilibrated sodium binding site in the C terminus of Kir3.1(N217D). **D**, Simulated structure for the equilibrated sodium binding site in the C terminus of Slack.

18.2 ± 3.9 mM (Fig. 3*E,F*). These results show that the Cl⁻ sensitivity of Slack could be changed modestly with increasing Na+ concentrations in the D818N background, suggesting either some contribution from additional Na+ regulatory sites or that the side chain of 818N could still play a role in coupling to Cl⁻ sensitivity, considering that D818A was not functional.

Theoretical and experimental binding affinities for Na+: comparison between the cytosolic domain of Kir3.1 and the predicted site in Slack

A homology model of the RCK2 domain of Slack was constructed, using as a template the structure of a prokaryotic RCK domain (Jiang et al., 2001) (Fig. 4*A*). We analyzed a 10 ns trajectory for the Na+-loaded Kir3.1N217D and Slack proteins in explicit solvent. Examples of the simulation system and ion binding pockets are shown in Figure 4*B–D*, respectively. The RMS fluctuations for heavy atoms were ~2 Å for both structures, indicating high stability for the MD simulations in both systems. The results for monovalent cation selectivity of the tentative binding sites located in the C terminus of the Kir3.1N217D and Slo2.2 channels are shown in Table 1. The sodium ion is stable residing in the tentative binding site for the entire course of the MD simulation (>10 ns for both systems), which is expected from reported experimental data indicating at least millimolar binding affinity to the tentative site (Sui et al., 1996; Ho and Murrell-Lagnado, 1999b). The site is open to solvent access, and water is transiently present in the first coordination shell of the ion. Our

Table 1. The relative free energy of Na+ selectivity of the binding site in the C terminus of Kir3.1N217D and wild-type Slo2.2

	$\Delta\Delta G_{Na+/K+}$	$\Delta\Delta G_{Na+/Li+}$
Kir3.1	2.9	1.1
Slo2.2	2.5	0.8
D818R	N/A	N/A
D818E	1.9	−0.2
D818N	1.1	4.9

All units are in kilocalories per moles. The positive sign in the relative free energy ($\Delta\Delta G$) refers to site preferences for Na+.

analysis indicates that the Na+ ion in the Slack site is coordinated by at least four residues and one water molecule (Fig. 4*D*). This partial hydration pattern is similar to that found in numerous previous reports on ion binding to external sites in the KcsA and NaK channels (Noskov and Roux, 2007). Both sites in the crystal and homology modeled structures display robust selectivity for Na+ against K+. This can be explained by the presence of a negatively charged residue such as D818 (Slo2.2) in the first coordination shell of the ion in agreement with the "field-strength" theory proposed in the mid-60s by George Eisenman (1962). A smaller cation such as Na+ would interact more favorably with the binding site containing charged ligand such as carboxylate (Eisenman, 1962; Noskov et al., 2004). In the absence of Na+, the interactions of K820 and D818 were stabilized through hydrogen bonding [an average distance of 1.8 ± 0.24 Å between the OD* (carboxylate oxygen)-HZ* (a hydrogen in a charged amino group)],
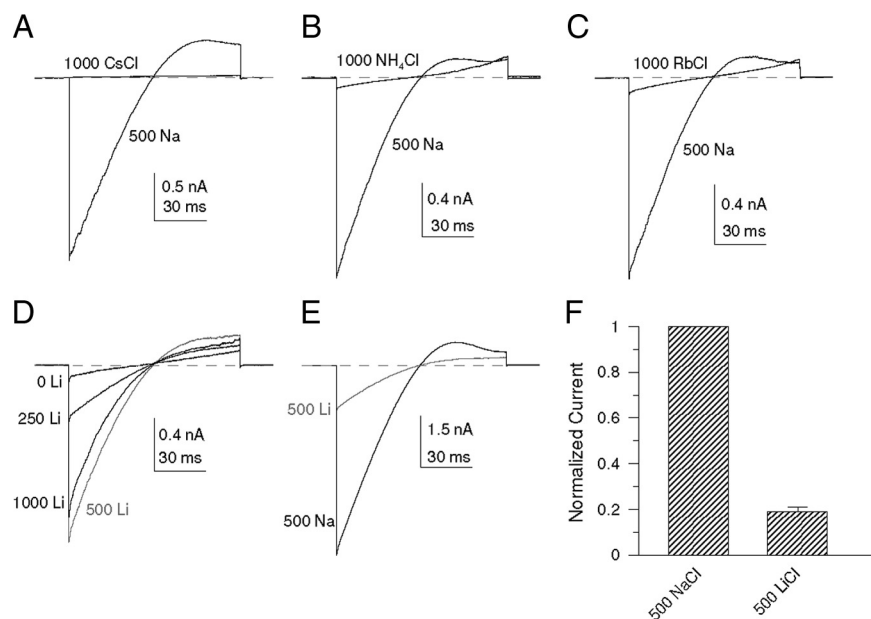
Figure 5. Li$^+$ activates the Slack channel in a dose-dependent manner. **A–C**, Typical current traces recorded in the inside-out patch configuration for Slack channel in Cs$^+$, NH$_{4+}$, and Rb$^+$, respectively. BS1 plus 1 M CsCl, 1 M NH$_4$Cl, and 1 M RbCl, respectively. The pipette solution included 90 mM KCl, 10 mM HEPES-K, and 5 mM EGTA-K. **D**, Current traces recorded with −100 to +100 mV ramp protocol in inside-out patch configuration. Bath solution includes 0–1000 mM LiCl. Other solution components were the same as indicated above. **E**, The same trace shown in **D** with 500 mM LiCl is shown in a different scale (gray) together with the trace recorded in 500 mM NaCl. **F**, Bar graph summaries showing the level of currents recorded in 500 mM LiCl relative to those recorded in 500 mM NaCl.
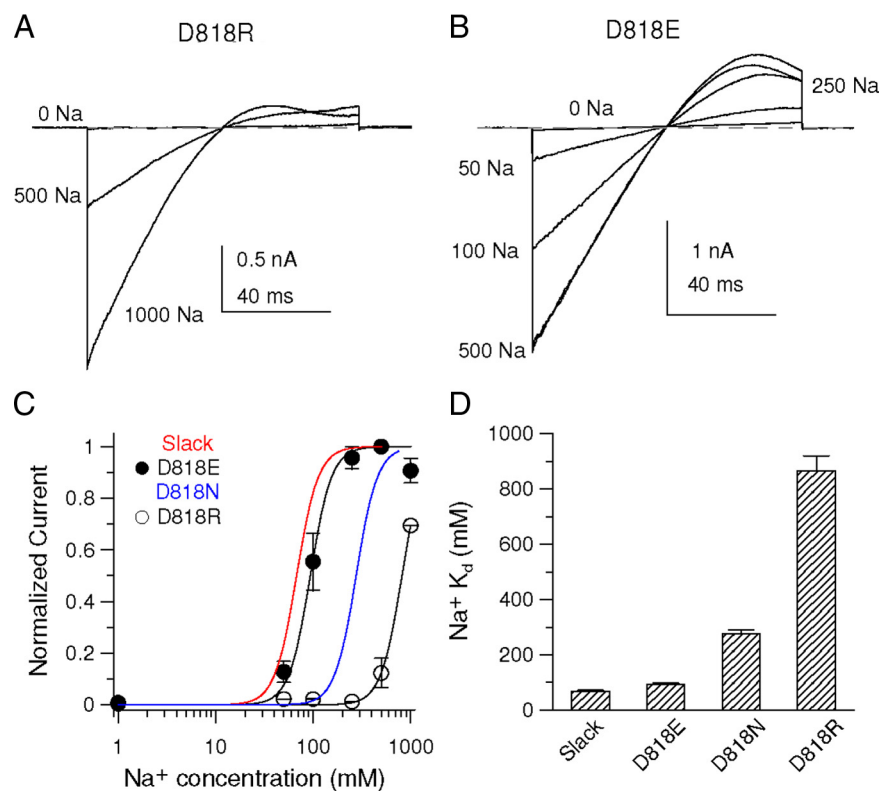
Figure 6. The D818R mutant shows a >10-fold decrease in Na$^+$ sensitivity, whereas the D818E mutant shows a similar Na$^+$ sensitivity to the wild-type Slack channel. **A**, **B**, Current traces recorded by ramp protocol from D818R and D818E, respectively. The bath solution was BS1. **C**, Sodium dose–response of D818E (K_d of 93 ± 4.5 mM, $n = 4$) and D818R (K_d of 866 ± 54 mM, $n = 4$). Data were fitted with the Hill equation. **D**, Bar graph summaries of K_d values of wild-type Slack and mutant channels (D818E, D818N, and D818R).

present in 92% of the frames with an average interaction energy of −92.3 kcal/mol). Na$^+$ destabilized this interaction between K820 and D818 (an average distance of 2.7 Å between the OD*-HZ*, present in ∼75% of the frames with an average interaction energy of −76.2 kcal/mol showing a large dispersion).

Our simulations on relative free energies of Na$^+$ versus Li$^+$ also predicted that this regulatory site in the C terminus of Slo2.2 can potentially be occupied by Li$^+$ but with weaker affinity than Na$^+$. The absolute binding affinities for a particular cation are difficult to calculate with FEP methods in part as a result of difficulties in sampling of ion dynamics for ending points of perturbation, in which the ion is fully uncoupled from the protein binding site (Deng and Roux, 2009; Mobley and Dill, 2009). At the same time, the accuracy in FEP results for monovalent cation affinity is known to be around ±1 kcal/mol and provides a robust measure of the difference in binding affinities between different cations (Noskov et al., 2004; Noskov and Roux, 2007). Li$^+$, unlike Na$^+$, was not stable in the site and tended to escape to the bulk solution. To prevent ion escape from the binding site, weak structural constraints were used in all simulations with an Li$^+$ ion. The ion was confined within a sphere with radius of 3.5 Å using a flat-bottom harmonic restraining potential with a force constant of 5 kcal/mol/Å (Noskov and Roux, 2007).

We proceeded to test for Li$^+$ effects in an electrophysiological experiment. The typical current traces recorded from inside-out patches using a voltage-ramp protocol in high concentrations of Cs$^+$, NH$_4^+$, or Rb$^+$ are shown in Figure 5A–C. None of these ions could significantly activate Slack currents in concentrations starting from 50 mM up to 1 M in macroscopic or unitary current recordings. Rb$^+$ is the ion most similar to K$^+$ and is often used in studies of selectivity. The lack of activation in the presence of Rb$^+$ is in good accord with the apparent Na$^+$ selectivity of the predicted binding site. Li$^+$ activated the Slack channel in a dose-dependent manner (Fig. 5D). Moreover, compared with Na$^+$, Li$^+$ exhibited a weaker potency in activating Slack currents (Fig. 5E). At a concentration of 500 mM, Li$^+$ activated Slack currents at ∼20% compared with Na$^+$ (Fig. 5E,F). These results were consistent with our predictions of constrained simulations evaluating Na$^+$/Li$^+$ selectivity of this site.

Because D818 is a negatively charged residue that can form electrostatic inter-
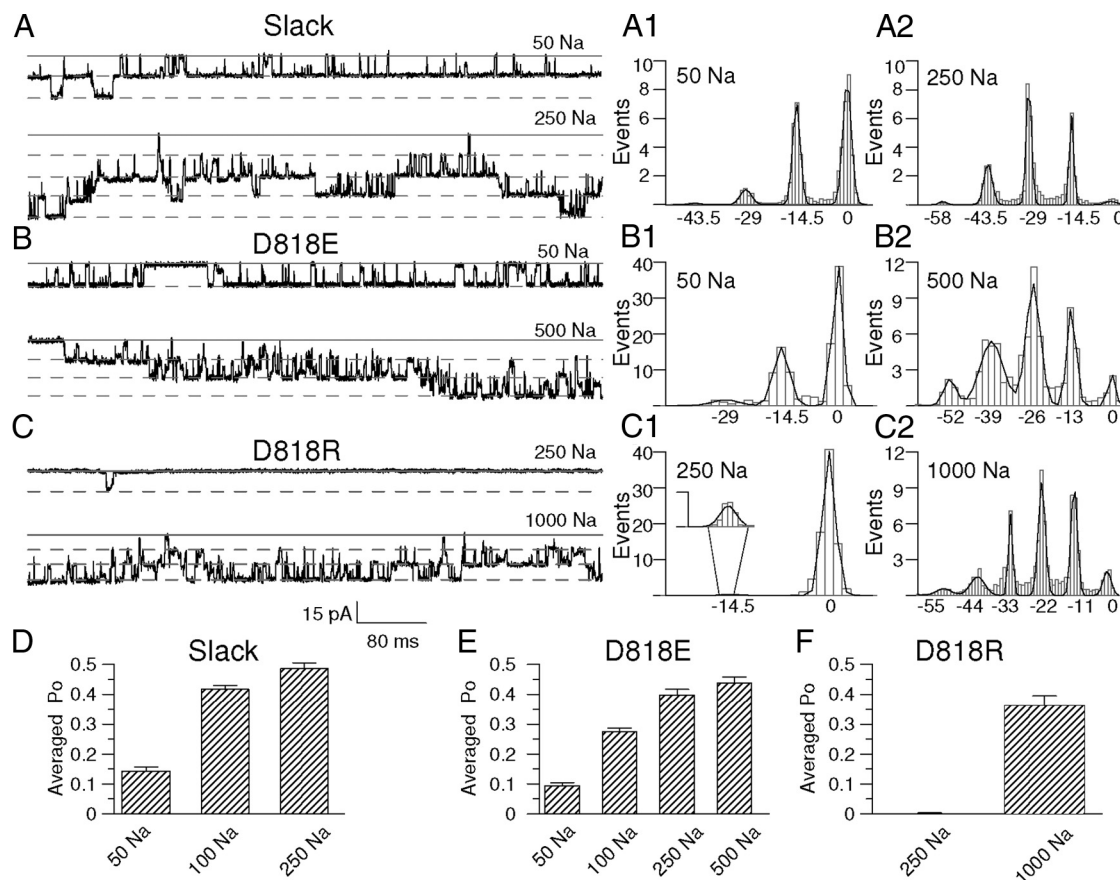
Figure 7. Na$^+$ sensitivity of unitary currents of wild-type Slack and D818E and D818R mutant channels. Sample single-channel traces measured at −100 mV at different Na$^+$ concentrations in the inside-out patch-clamp configuration for wild-type Slack. ***A***, D818E; ***B***, D818R; ***C***, total events were fitted by a Gaussian functions. ***A1***, Slack with 50 mM Na$^+$; ***A2***, Slack with 250 mM Na$^+$; ***B1***, D818E with 50 mM Na$^+$; ***B2***, D818E with 500 mM Na$^+$; ***C1***, D818R with 250 mM Na$^+$; ***C2***, D818R with 1000 mM Na$^+$. Each number in the y-axis is times 10,000 events. The unit in the y-axis of the ***C1*** inset stands for 4000 events. x-axes labels show the current level in picoamperes. Averaged P_o values in different sodium concentrations of Slack (50 mM Na$^+$, P_o = 0.14 ± 0.013; 100 mM Na$^+$, P_o = 0.42 ± 0.014; 250 mM Na$^+$, P_o = 0.48 ± 0.02), D818E (50 mM Na$^+$, P_o = 0.09 ± 0.01; 100 mM Na$^+$, P_o = 0.27 ± 0.014; 250 mM Na$^+$, P_o = 0.4 ± 0.02; 500 mM Na$^+$, P_o = 0.44 ± 0.02), and D818R (250 mM Na$^+$, P_o = 0.002 ± 0.001; 1000 mM Na$^+$, P_o = 0.36 ± 0.03) were summarized in ***D***, ***E***, and ***F***, respectively.

actions with positive charges, such as in Li$^+$ and Na$^+$, we tested whether this electrostatic interaction plays a major role in the binding with Na$^+$. The results of FEP simulations on Slack mutants are shown also in Table 1. Neutralization of the charge in position 818 by mutating the aspartate to an asparagine had a notable impact on the stability of bound sodium ion in the binding site as well as on the selectivity for Na$^+$. The reversal of the charge (D/R) mutation led to a very unstable binding site and large harmonic constraints (100 kcal/mol/Å^2) were required to keep the ion in the site. At the same time, a mutation conserving the charge (D/E) had no statistically significant effects on the ion selectivity of this binding site in free energy simulations.

We followed up to experimentally test the predictions of the FEP simulations for the D818 mutants. The D818R mutation further decreased Slack sensitivity to Na$^+$ compared with D818N. With 500 mM Na$^+$, channel activation was still very low, but with 1M Na$^+$, it showed a significant increase still not reaching the maximum (Fig. 6*A*). Hill equation fits gave an estimate of the K_d for D818R of ∼866 ± 154 mM (keeping the Hill equation coefficient factor as 4 and using the largest fitted current as 1 to normalize different macropatches) (Fig. 6*C*). In contrast, when the negative charge was retained by mutating the D to E, the K_d was only slightly higher than wild type (EC$_{50}$ of 80 ± 10 mM) (Fig. 6*B*,*C*). The bar graph shown in Figure 6*D* summarizes the K_d values for mutations at this site.

We further tested the Na$^+$ sensitivity of the wild-type Slack, D818E, and D818R at the single-channel level at −100 mV. No differences in unitary conductance were observed among the wild-type Slack and the mutants D818E and D818R. The unitary conductance of these channels in ND96 was ∼145 pS, consistent with previously reported results (Yuan et al., 2003; Chen et al., 2009). The open probability of these channels increased with increasing Na$^+$ concentrations (Fig. 7*A–C*). As shown in the sample traces, the wild-type channel (at 250 mM Na$^+$) and the D818E mutant (at 500 mM Na$^+$) exhibited saturated nP_o values of 1.64 and 1.72, respectively, whereas there were a total of four discrete observed channel levels. However, for D818R, the saturated nP_o was 1.82 (1000 mM Na) when there were a total of five discrete observed channel levels. The averaged P_o from different patches was calculated by using the largest number of simultaneously open channels that was seen in the records. The saturated P_o of Slack and D818E was 0.48 ± 0.02 and 0.44 ± 0.02, respectively, whereas the saturated P_o of D818R was 0.36 ± 0.03 (Fig. 7*D–F*). These results show that D818R saturated open probability is still lower than that of D818E or the wild-type Slack even when the patches were perfused with much higher concentrations of Na$^+$. These results of the unitary activity of Slack were consistent with those obtained from macropatch recordings and FEP simulations.

Discussion

It has been shown previously that three Kir channels (Kir3.2, Kir3.4, and Kir5.1) possess an Na$^+$ sensor that endows them with Na$^+$ sensitivity even in heteromeric assemblies they form with other channel subunits that lack the Na$^+$ sensor (Rosenhouse-Dantsker et al., 2008). MD simulations and mutagenesis experiments, based on crystallographic structures, showed that the Kir Na$^+$ sensor partly comprises the side chains of an aspartate and a histidine that are located across from one another in a cytosolic loop (Rosenhouse-Dantsker et al., 2008). This part of the coordination site forms a motif found in the three Na$^+$-sensitive Kir channels, DXRXXH, which can operate even in Na$^+$-insensitive Kir channels, when engineered by mutagenesis (e.g., Kir3.1N217D or Kir2.1N216D) (Ho and Murrell-Lagnado, 1999a; Zhang et al., 1999). In the current study, screening the C terminus of Slo2.2 for the presence of this Na$^+$-sensing motif revealed several possible sites, and mutagenesis confirmed that one such motif localized in the RCK2 domain of Slo2.2 operated as an Na$^+$ sensor. Again the aspartate and the histidine side chains were key elements of the Slo2.2 Na$^+$ coordination site. Free energy calculations were also consistent with experimental data regarding cation selectivity or the behavior of mutants of the critical Asp (D818E, D818N, and D818R). These results provide compelling evidence that a conserved local structural element of an Na$^+$ sensor is used by distinct potassium channels with different general structures.

For Kir channels, mutation of the conserved arginine residue in the Na$^+$-sensing motif greatly reduced channel activity. Indeed, this Arg residue has been shown by a number of studies and in different Kir channels to be critical for interactions with phosphatidylinositol-bisphosphate (PIP$_2$) and its mutation to inhibit activity and cause the condition known as Andersen's syndrome (e.g., for Kir2.1, R218Q or R218W) (Zhang et al., 1999; Lopes et al., 2002; Pegan et al., 2005). In the absence of Na$^+$, the Asp could hydrogen bond with the Arg and prevent it from interacting with PIP$_2$, thus keeping the channel inactive. In the presence of Na$^+$, however, the Asp would switch to coordinate the Na$^+$ ion, thus leaving the Arg free to interact with PIP$_2$ and activate the channel (Rosenhouse-Dantsker et al., 2008). In the Slo2.2 channel, there is a lysine in place of the Arg residue in the Na$^+$-sensing motif. Mutation of K820 did not affect Na$^+$ sensitivity of Slo2.2 channels. However, like in Kir channels, the Slo2.2 K820 residue hydrogen bonds with D818 in the absence of Na$^+$, whereas in the presence of Na$^+$, this interaction is destabilized. The functional significance of this switching mechanism is not presently clear for Slo2.2 channels.

However, the mere location of the Na$^+$-sensing motif in the RCK2 domain is intriguing. The RCK (regulators of conductance of K$^+$) domains are specialized intracellular structures found in many putative prokaryotic K$^+$ channels. The structure of the Ca^{2+}-modulated bacterial channel MthK suggested formation of a gating ring composed of RCK1 and RCK2 domains, in which binding of Ca^{2+} was proposed to expand the ring, pull on the linkers that connected it to the channel gates, and thus open the channel (Jiang et al., 2002a). Similar models have been proposed for Slo1 channels (Niu et al., 2004), because Ca^{2+} and Mg^{2+} binding sites to the RCK1 domain have been reported (Xia et al., 2002) and have been shown to contribute significantly to Ca^{2+} sensitivity by a large number of studies (Salkoff et al., 2006; Cui et al., 2009). Thus, although additional important Ca^{2+}-sensing sites have been identified, the contribution of the RCK1 domain to Ca^{2+} sensitivity is widely accepted. Our finding that yet another ion sensor, the Slo2.2 Na$^+$ sensor, is localized in the RCK2 domain of this channel provides additional credit to the notion that RCK domains are designed to couple distinct ion-sensing mechanisms to channel gating. Parallels with the Slo1 design of ion sensitivity may exist in Slo2.2 as well. Although mutations of the Asp and His residues in the identified RCK2 site were detrimental to Na$^+$ sensitivity, they did not abolish it, suggesting that additional sites may be involved in sensing Na$^+$. Additional studies will be required, as has been the case with the Slo1 channels, to define the relationship of the RCK2 site to potential other ones and to discern how they couple to the channel gate. Finally, Slo2 channels show synergistic activation by both Na$^+$ and Cl$^-$. Although the elimination of the RCK2 Na$^+$ site affected Na$^+$ sensitivity independently of the presence of Cl$^-$, at the same time it greatly diminished the ability of Cl$^-$ to activate the channel. Thus, the RCK2 Na$^+$ site controls Cl$^-$ sensitivity but is not controlled by Cl$^-$ itself. This in an important constraint to consider as future studies aim to unravel the intricate interdependence of Slo2.2 on Na$^+$ and Cl$^-$.

The physiological roles of Na$^+$-sensitive channels continue to be increasingly appreciated. In heart, K$_{Na}$ may play an important protective role under ischemic conditions (Kameyama et al., 1984; Luk and Carmeliet, 1990; Mitani and Shattock, 1992). In neurons, their effects maybe dependent on a concomitant Na$^+$ influx (Dryer, 1994), because they appear to be significant components of outward K$^+$ currents (Budelli et al., 2009), to regulate the accuracy of timing of auditory neurons (Yang et al., 2007), and to modulate rhythmic firing and adaptation (Brown et al., 2008). In kidney, Slo2.2 has been shown to be expressed in the medullary and cortical thick ascending limb of Henle's loop, one of the Na$^+$ reabsorbing segments of the nephron (Paulais et al., 2006). Interestingly, the remaining Na$^+$ reabsorbing segments of the nephron, the proximal and distal convoluted tubules, express the inwardly rectifying Kir5.1 Na$^+$-sensitive channel. Thus, each Na$^+$ reabsorbing segment of the nephron possesses an Na$^+$-activated K$^+$ channel. Because a negative membrane potential of kidney tubular cells would contribute substantially toward Na$^+$ reabsorption from the tubular lumen into the cell, Na$^+$-sensitive K$^+$ channels could ensure that the membrane potential is maintained near the equilibrium potential for potassium. However, the purpose of using Slo2.2 versus Kir5.1 in specific nephron segments to achieve a negative membrane potential is likely to depend on characteristics of the individual channels rather than their similar Na$^+$-sensing mechanism.

References

Bennett-Lovsey RM, Herbert AD, Sternberg MJ, Kelley LA (2008) Exploring the extremes of sequence/structure space with ensemble fold recognition in the program Phyre. Proteins 70:611–625.

Bhattacharjee A, Gan L, Kaczmarek LK (2002) Localization of the Slack potassium channel in the rat central nervous system. J Comp Neurol 454:241–254.

Bhattacharjee A, Joiner WJ, Wu M, Yang Y, Sigworth FJ, Kaczmarek LK (2003) Slick (Slo2.1), a rapidly-gating sodium-activated potassium channel inhibited by ATP. J Neurosci 23:11681–11691.

Brooks BR, Bruccoleri RE, Olafson BD, States DJ, Swaminathan S, Karplus M (1983) Charmm: a program for macromolecular energy, minimization, and dynamics calculations. J Comput Chem 4:187–217.

Brown MR, Kronengold J, Gazula VR, Spilianakis CG, Flavell RA, von Hehn CA, Bhattacharjee A, Kaczmarek LK (2008) Amino-termini isoforms of the Slack K$^+$ channel, regulated by alternative promoters, differentially modulate rhythmic firing and adaptation. J Physiol 586:5161–5179.

Budelli G, Hage TA, Wei A, Rojas P, Jong YJ, O'Malley K, Salkoff L (2009) Na$^+$-activated K$^+$ channels express a large delayed outward current in neurons during normal physiology. Nat Neurosci 12:745–750.

Caplan DA, Subbotina JO, Noskov SY (2008) Molecular mechanism of ion–

ion and ion–subtrate coupling in the NA+-dependent leucine trasportor LeuT. Biophys J 95:4613–4621.

Chen H, Kronengold J, Yan Y, Gazula VR, Brown MR, Ma L, Ferreira G, Yang Y, Bhattacharjee A, Sigworth FJ, Salkoff L, Kaczmarek LK (2009) The N-terminal domain of Slack determines the formation and trafficking of Slick/Slack heteromeric sodium-activated potassium channels. J Neurosci 29:5654–5665.

Cui J, Yang H, Lee US (2009) Molecular mechanisms of BK channel activation. Cell Mol Life Sci 66:852–875.

Deng Y, Roux B (2009) Computations of standard binding free energies with molecular dynamics simulations. J Phys Chem B 113:2234–2246.

Dryer SE (1994) Na$^+$-activated K$^+$ channels: a new family of large-conductance ion channels. Trends Neurosci 17:155–160.

Egan TM, Dagan D, Kupper J, Levitan IB (1992) Na$^+$-activated K$^+$ channels are widely distributed in rat CNS and in *Xenopus* oocytes. Brain Res 584:319–321.

Eisenman G (1962) Cation selective electrodes and their mode of operation. Biophys J 2:259–323.

Essmann U, Perera L, Berkowitz ML, Darden T, Lee H, Pedersen LG (1995) A smooth particle mesh Ewald method. J Chem Phys 103:8577–8593.

Feller SE, Zhang YH, Pastor RW, Brooks BR (1995) Constant-pressure molecular-dynamics simulation: the Langevin piston method. J Chem Phys 103:4613–4621.

Gao SB, Wu Y, Lü CX, Guo ZH, Li CH, Ding JP (2008) Slack and Slick KNa channels are required for the depolarizing afterpotential of acutely isolated, medium diameter rat dorsal root ganglion neurons. Acta Pharmacol Sin 29:899–905.

Ho IH, Murrell-Lagnado RD (1999a) Molecular determinants for sodium-dependent activation of G protein-gated K$^+$ channels. J Biol Chem 274:8639–8648.

Ho IH, Murrell-Lagnado RD (1999b) Molecular mechanism for sodium-dependent activation of G protein-gated K$^+$ channels. J Physiol 520:645–651.

Jiang Y, Pico A, Cadene M, Chait BT, MacKinnon R (2001) Structure of the RCK domain from the *E. coli* K$^+$ channel and demonstration of its presence in the human BK channel. Neuron 29:593–601.

Jiang Y, Lee A, Chen J, Cadene M, Chait BT, MacKinnon R (2002a) Crystal structure and mechanism of a calcium-gated potassium channel. Nature 417:515–522.

Jiang Y, Lee A, Chen J, Cadene M, Chait BT, MacKinnon R (2002b) The open pore conformation of potassium channels. Nature 417:523–526.

Jin T, Peng L, Mirshahi T, Rohacs T, Chan KW, Sanchez R, Logothetis DE (2002) The (beta)gamma subunits of G proteins gate a K$^+$ channel by pivoted bending of a transmembrane segment. Mol Cell 10:469–481.

Jo S, Lim JB, Klauda JB, Im W (2009) CHARMM-GUI membrane builder for mixed bilayers and its application to yeast membranes. Biophys J 97:50–58.

Kameyama M, Kakei M, Sato R, Shibasaki T, Matsuda H, Irisawa H (1984) Intracellular Na$^+$ activates a K$^+$ channel in mammalian cardiac cells. Nature 309:354–356.

Krivov GG, Shapovalov MV, Dunbrack RL Jr (2009) Improved prediction of protein side-chain conformations with SCWRL4. Proteins 77:778–795.

Kumar S, Bouzida D, Swendsen RH, Kollman PA, Rosenberg JM (1992) The weighted histogram analysis method for free-energy calculations on biomolecules. 1. The method. J Comput Chem 13:1011–1021.

Lopes CM, Zhang H, Rohacs T, Jin T, Yang J, Logothetis DE (2002) Alterations in conserved Kir channel-PIP2 interactions underlie channelopathies. Neuron 34:933–944.

Luk HN, Carmeliet E (1990) Na+-activated K$^+$ current in cardiac cells: rectification, open probability, block and role in digitalis toxicity. Pflugers Arch 416:766–768.

Luzhkov VB, Aqvist J (2001) K$^+$/Na$^+$ selectivity of the KcsA potassium channel from microscopic free energy perturbation calculations. Biochim Biophys Acta 1548:194–202.

Luzhkov VB, Almlöf M, Nervall M, Aqvist J (2006) Computational study of the binding affinity and selectivity of the bacterial ammonium transporter AmtB. Biochemistry 45:10807–10814.

Mitani A, Shattock MJ (1992) Role of Na-activated K channel, Na-K-Cl cotransport, and Na-K pump in [K]e changes during ischemia in rat heart. Am J Physiol 263:H333–H340.

Mobley DL, Dill KA (2009) Binding of small-molecule ligands to proteins: "what you see" is not always "what you get." Structure 17:489–498.

Nanou E, El Manira A (2007) A postsynaptic negative feedback mediated by coupling between AMPA receptors and Na$^+$-activated K$^+$ channels in spinal cord neurones. Eur J Neurosci 25:445–450.

Nanou E, Kyriakatos A, Bhattacharjee A, Kaczmarek LK, Paratcha G, El Manira A (2008) Na$^+$-mediated coupling between AMPA receptors and KNa channels shapes synaptic transmission. Proc Natl Acad Sci U S A 105:20941–20946.

Niu X, Qian X, Magleby KL (2004) Linker-gating ring complex as passive spring and Ca^{2+}-dependent machine for a voltage- and Ca^{2+}-activated potassium channel. Neuron 42:745–756.

Noskov SY, Roux B (2007) Importance of hydration and dynamics on the selectivity of the KcsA and NaK channels. J Gen Physiol 129:135–143.

Noskov SY, Roux B (2008) Control of ion selectivity in LeuT: two Na+ binding sites with two different mechanisms. J Mol Biol 377:804–818.

Noskov SY, Bernèche S, Roux B (2004) Control of ion selectivity in potassium channels by electrostatic and dynamic properties of carbonyl ligands. Nature 431:830–834.

Paulais M, Lachheb S, Teulon J (2006) A Na$^+$- and Cl$^-$-activated K$^+$ channel in the thick ascending limb of mouse kidney. J Gen Physiol 127:205–215.

Pegan S, Arrabit C, Zhou W, Kwiatkowski W, Collins A, Slesinger PA, Choe S (2005) Cytoplasmic domain structures of Kir2.1 and Kir3.1 show sites for modulating gating and rectification. Nat Neurosci 8:279–287.

Rosenhouse-Dantsker A, Logothetis DE (2006) New roles for a key glycine and its neighboring residue in potassium channel gating. Biophys J 91:2860–2873.

Rosenhouse-Dantsker A, Sui JL, Zhao Q, Rusinova R, Rodríguez-Menchaca AA, Zhang Z, Logothetis DE (2008) A sodium-mediated structural switch that controls the sensitivity of Kir channels to PtdIns(4,5)P(2). Nat Chem Biol 4:624–631.

Salkoff L, Butler A, Ferreira G, Santi C, Wei A (2006) High-conductance potassium channels of the SLO family. Nat Rev Neurosci 7:921–931.

Souaille M, Roux B (2001) Extension to the weighted histogram analysis method: combining umbrella sampling with free energy calculations. Comput Phys Commun 135:40–57.

Sui JL, Chan KW, Logothetis DE (1996) Na$^+$ activation of the muscarinic K$^+$ channel by a G-protein-independent mechanism. J Gen Physiol 108:381–391.

Tamsett TJ, Picchione KE, Bhattacharjee A (2009) NAD+ activates KNa channels in dorsal root ganglion neurons. J Neurosci 29:5127–5134.

Xia XM, Zeng X, Lingle CJ (2002) Multiple regulatory sites in large-conductance calcium-activated potassium channels. Nature 418:880–884.

Yang B, Desai R, Kaczmarek LK (2007) Slack and Slick K(Na) channels regulate the accuracy of timing of auditory neurons. J Neurosci 27:2617–2627.

Yuan A, Santi CM, Wei A, Wang ZW, Pollak K, Nonet M, Kaczmarek L, Crowder CM, Salkoff L (2003) The sodium-activated potassium channel is encoded by a member of the Slo gene family. Neuron 37:765–773.

Zeng XH, Xia XM, Lingle CJ (2005) Divalent cation sensitivity of BK channel activation supports the existence of three distinct binding sites. J Gen Physiol 125:273–286.

Zhang H, He C, Yan X, Mirshahi T, Logothetis DE (1999) Activation of inwardly rectifying K$^+$ channels by distinct PtdIns(4,5)P2 interactions. Nat Cell Biol 1:183–188.